

Helium-helium clustering states in ^{12}Be

Z. H. Yang,¹ Y. L. Ye,^{1,*} Z. H. Li,¹ J. L. Lou,¹ J. S. Wang,² D. X. Jiang,¹ Y. C. Ge,¹ Q. T. Li,¹ H. Hua,¹ X. Q. Li,¹ F. R. Xu,¹ J. C. Pei,¹ R. Qiao,¹ H. B. You,¹ H. Wang,^{1,3} Z. Y. Tian,¹ K. A. Li,^{1,2} Y. L. Sun,¹ H. N. Liu,^{1,3} J. Chen,¹ J. Wu,^{1,3} J. Li,¹ W. Jiang,¹ C. Wen,^{1,3} B. Yang,¹ Y. Liu,¹ Y. Y. Yang,² P. Ma,² J. B. Ma,² S. L. Jin,² J. L. Han,² and J. Lee³

¹State Key Laboratory of Nuclear Physics and Technology, School of Physics, Peking University, Beijing 100871, China

²Institute of Modern Physics, Chinese Academy of Science, Lanzhou 730000, China

³RIKEN Nishina Center, 2-1 Hirosawa, Wako, Saitama 351-0198, Japan

(Received 15 December 2014; published 6 February 2015)

An inelastic excitation experiment was performed with a ^{12}Be beam at 29 MeV/u on a carbon target. New resonances close to the respective cluster separation thresholds were observed in ^{12}Be for the $^4\text{He} + ^8\text{He}$ and $^6\text{He} + ^6\text{He}$ decay channels, confirming the previously proposed molecular rotational bands. Using the model-independent angular correlation analysis, a 0^+ spin parity is assigned to the remarkably large peak at 10.3 MeV in the $^4\text{He} + ^8\text{He}$ channel. A distorted wave Born approximation (DWBA) calculation was compared to the experimental differential cross section of this state, resulting in a largely enhanced monopole transition matrix element of $7.0 \pm 1.0 \text{ fm}^2$, in good agreement with the generalized two-center cluster model (GTCM) prediction assuming a preformed α - $4n$ - α configuration. Together with the previously reported large cluster spectroscopic factor, the strong clustering in ^{12}Be is well demonstrated. The detection focused on the most forward angles, by using a zero-deg telescope, is essential in the present measurement.

DOI: [10.1103/PhysRevC.91.024304](https://doi.org/10.1103/PhysRevC.91.024304)

PACS number(s): 21.60.Gx, 25.60.Dz, 25.70.Ef, 25.70.Mn

I. INTRODUCTION

The cluster formation in nuclei is one of the most interesting phenomena and has been investigated since early in the history of nuclear physics [1,2]. Intuitively, the effect of nuclear clustering could be inferred from the disintegration of heavy nuclei via the emission of α particles or heavier fragments like ^{14}C , which are most likely pre-formed inside the mother nucleus [3,4]. Many theoretical and experimental efforts have been devoted to studies on the cluster structure, but a full understanding of this phenomenon and related dynamics are still far from settled [5,6]. Elucidating the mechanism of clustering in nuclei is of fundamental importance not only for nuclear many-body dynamics but also for understanding some key processes in nuclear astrophysics [5,7].

In 1968 Ikeda *et al.* proposed a threshold rule for cluster formation in stable nuclei, as illustrated in the well-known Ikeda diagram [8]. They speculated that at the vicinity of an energy threshold for cluster separation, the nucleus tends to expand its size and favor the cluster formation in consequence [8,9]. As a matter of fact, the increasing binding (tightness) of the cluster with the decreasing environmental matter density has been experimentally justified recently in heavy-ion collisions [10]. Owing to the worldwide development of radioactive ion beam facilities and relevant detection techniques, studies on the cluster structure have been extended to unstable nuclei [5,11,12]. Clustering phenomenon is expected to be enhanced for nuclei far from the stability line, since the low density surface might be formed more easily even in their ground states [13,14].

In the early times, studies of the cluster structure were focused on the dinuclear cluster systems by means of measuring

some narrow resonances, the so-called molecular resonances, populated in, for instance, $^{12}\text{C} + ^{12}\text{C}$ and alike collisions [15]. From the energy-spin systematics of these resonances, rotational bands with large moments of inertia, indicative of large deformations, were constructed. An extremely large moment of inertia was then proposed as one of the necessary criteria for the identification of a cluster state [15,16]. However, as has been emphasized recently, although the large deformation is a strong signal of cluster formation, it falls short of being conclusive [6]. Another argument, the partial width for cluster decay, is of primary importance as well [6,17]. Recently the abnormally large monopole transition strength has also been proposed as an “imprint” of clustering in light nuclei [18–20].

The cluster structure in Be isotopes has gathered much attention in recent years, for their unique two-center symmetric system built on a well-established $\alpha + \alpha$ rotor surrounded by a few valence neutrons [21–24]. Indeed the quenching of the $N = 8$ shell closure in ^{12}Be , observed in various experiments [25–28], can be well explained within an α - $4n$ - α cluster model [22,23,29]. Impressive progress on this topic has been made from the theoretical side, including antisymmetrized molecular dynamics (AMD) [30], the generator coordinate method (GCM) [31], and the generalized two-center cluster model (GTCM) [22–24]. In the meantime the related experimental measurements are very limited until now and the results are sometimes inconsistent with each other. In Ref. [32,33], Freer *et al.* reported the inelastic scattering of ^{12}Be off proton and carbon targets at 31.5 MeV/u. Some molecular resonant (MR) states (4^+ , 6^+ , and 8^+) were observed, from which a $^6\text{He} + ^6\text{He}$ molecular rotational band was constructed, possessing a large moment of inertia in accordance with the α - $4n$ - α cluster structure in ^{12}Be . Soon after, Charity *et al.* repeated this kind of measurements at a higher incident energy (50 MeV/nucleon) [34]. Unexpectedly, most of the resonances, reported by Freer *et al.*, could not be reproduced in this

*Corresponding author: yeyl@pku.edu.cn

work, although higher statistics were accumulated [34]. Meanwhile, hints of MR states in ^{12}Be were also reported in some other measurements [35–37]. It is worth noting that the low-lying 0^+ and 2^+ MR states were missed in the experiments of Freer *et al.* and Charity *et al.*, owing to the noncoverage of the detectors around zero degrees, resulting in a very low detection efficiency at small decay energies.

Following the previous brief report [18], we give here the details associated with a newly performed breakup experiment for ^{12}Be , concentrating on the detection at most forward angles [18]. This measurement aims not only to complement the molecular rotational bands, but in particular to investigate the monopole transition strength, which was quantitatively predicted in the GTCM approach, in order to pin down the cluster structure in ^{12}Be [19]. This paper is organized as follows. In Sec. II, the experimental setup and detection technique are described. Section III is dedicated to the experimental results and discussions, and a brief summary is presented in Sec. IV.

II. EXPERIMENTAL DETAILS

The present measurements were carried out at the Radioactive Ion Beam Line at Heavy Ion Research Facility in Lanzhou (HIRFL-RIBLL) [38]. A secondary beam of ^{12}Be at 29 MeV/nucleon, with an intensity of ~ 3000 particles per second (pps), was produced from fragmentation of a 70 MeV/u ^{18}O primary beam on a thick ^9Be target. The beam particle identification was realized event by event using the measured time-of-flight (TOF) and energy loss (ΔE) values. The purity for ^{12}Be is about 70%. A schematic view of the experimental setup is given in Fig. 1. The secondary ^{12}Be beam was tracked onto a 100-mg/cm 2 carbon target by two parallel plate avalanche chambers (PPACs) with position resolutions (FWHM) of about 1 mm in both X and Y directions. A downstream zero-degree telescope was employed to record the charged fragments, which consists of a 300- μm -thick double-sided silicon strip detector (DSSD) and a 1500- μm -thick large-size silicon detector (SSD), followed by a 4×4 CsI(Tl) scintillator array. The DSSD has an active area of 6.4 cm \times 6.4 cm with front and back faces each divided into 32 strips, providing a position resolution of 2 mm in both X or Y directions. It was placed at 15.5 cm from the target, covering an angular range of 0–12 $^\circ$ in the laboratory system.

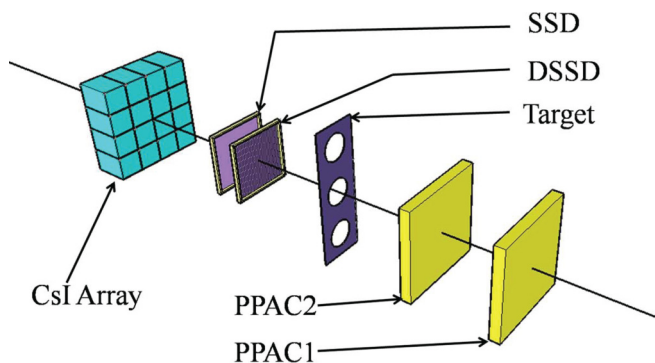


FIG. 1. (Color online) Schematic view of the experimental setup.

Each CsI(Tl) unit has a thickness of 3 cm and a front face of 2.5 cm \times 2.5 cm and was read out by a photodiode. The CsI(Tl) array was installed at 32.3 cm from the target so as to cover the similar angular range of the DSSD.

The energy calibration of the CsI(Tl) scintillators was achieved by using secondary ^6He beams at 25 and 35 MeV/nucleon, and ^4He beams at 30, 40, and 50 MeV/nucleon, produced from the same primary beam. Although some nonlinear responses have been reported in the literature, a linear formula can be a good approximation for light ions like He isotopes with deposited energies higher than ~ 80 MeV [33]. In our case a good linear energy response was extracted for the CsI(Tl) light output, with an energy resolution (FWHM) of $\sim 3\%$ for ^4He particles at 50 MeV/nucleon. These beams with known energies were also used to calibrate the DSSD. The newly developed self-calibration method was applied to match the energies detected by different strips and therefore to improve the overall resolution [39]. An energy resolution of 46 KeV (0.86% in FWHM) for the 5.486-MeV α particles from the ^{241}Am source was achieved.

In the present work, only events with two charged fragments detected by the telescope in coincidence (multiplicity 2) were recorded. The relative energy (E_{rel}) of a pair of fragments was reconstructed from their kinetic energies (T_a, T_b) and the opening angle (θ). According to the invariant mass method as used in our previous work, the excitation energy of a resonance is expressed as [40–42]

$$\begin{aligned} E_x &= E_{\text{rel}} + E_{\text{thres}}, \\ E_{\text{rel}} &= \sqrt{M^2} - M_a - M_b, \\ M^2 &= M_a^2 + M_b^2 + 2(M_a + T_a)(M_b + T_b) \\ &\quad - 2\sqrt{(T_a^2 + 2T_a M_a)(T_b^2 + 2T_b M_b)} \cos\theta, \end{aligned} \quad (1)$$

where E_{thres} is the threshold energy (or separation energy) of the corresponding cluster decay.

Monte Carlo simulations were performed to determine the resolution of the reconstructed excitation energy and the detection efficiency for the $2\text{-}^X\text{He}$ events. The simulation takes into account the reaction position and energy loss in the target, and the energy and position resolutions of the detectors. For ^{12}Be decaying into the $^6\text{He} + ^6\text{He}$ and $^4\text{He} + ^8\text{He}$ channels, the resolution (FWHM) is determined to be around 0.4 MeV at a relative energy (E_{rel}) of 1 MeV and increases to about 0.8 MeV at an E_{rel} of 4 MeV [43], mainly attributed to the uncertainty of the interaction depth in the target. The detection efficiency is mainly limited by the configuration of the CsI(Tl) scintillator array. If the relative energy of the two fragments (E_{rel}) is very small, they will mostly hit the same CsI(Tl) unit and lose the event identity. On the other hand if E_{rel} is too large, one or both of the fragments may escape from the array with appreciable probabilities. The detection efficiency for ^{12}Be decaying into the $^4\text{He} + ^8\text{He}$ channel is shown in Fig. 2, with a maximum value of $\sim 49\%$ at small E_{rel} , which decreases to $\sim 30\%$ at $E_{\text{rel}} = 3$ MeV. Similar detection efficiency is also found for other decay channels, such as $^6\text{He} + ^6\text{He}$. The zero-deg telescope employed in the present measurement, with fine pixels and an angular coverage focusing on the most forward angles, offered a remarkably higher sensitivity

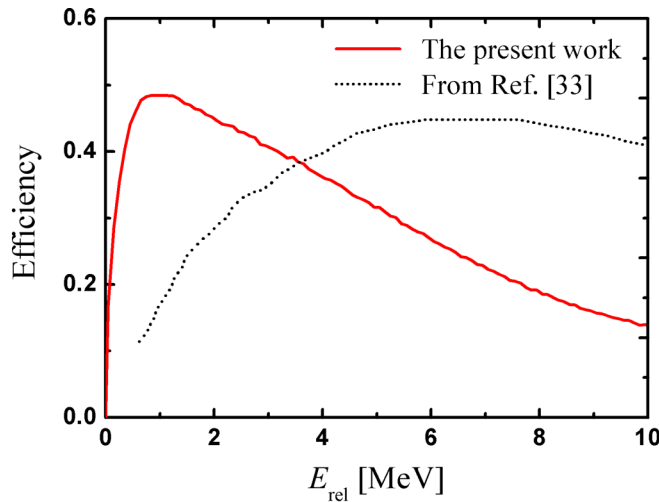


FIG. 2. (Color online) The detection efficiency of the present work for ^{12}Be decaying into the $^4\text{He} + ^8\text{He}$ channel (red [gray] solid line). For comparison, the efficiency curve from Freer's experiment [32] is also plotted (black dotted line).

for near-threshold resonant states compared to the previously applied detector systems [32,34], as illustrated in Fig. 2.

III. RESULTS AND DISCUSSION

From the characteristic energy loss in the DSSD + CsI(Tl) telescope, ^4He , ^6He , and ^8He isotopes are unambiguously identified as shown in Fig. 3. Events with two helium fragments coincidentally detected by the telescope were selected based on the pixelation of the telescope, and used to reconstruct the relative energy according to Eq. (1). The reconstruction procedure was first checked with $^4\text{He} + ^4\text{He}$ coincident events. A sharp peak close to 100 KeV was clearly reproduced, which corresponds to the ground state of ^8Be with a decay energy of 92 KeV [44]. The background counting was achieved by carrying out measurements with empty target, in which no reasonable yields were observed for multiplicity-2 events. This demonstrates that the coincident measurement is very effective to reduce the background contamination, even for detection around the beam direction.

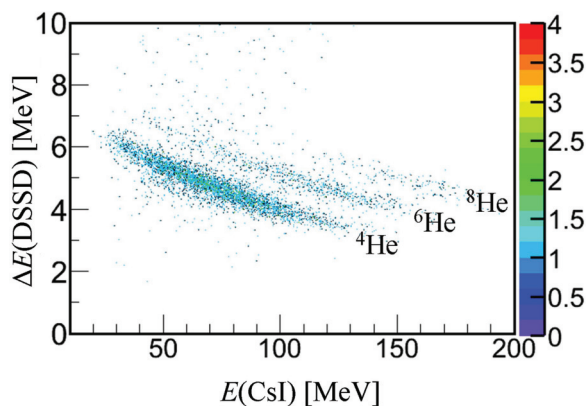


FIG. 3. (Color online) Particle identification (PID) spectrum for multiplicity-2 events resulted from the ^{12}Be breakup.

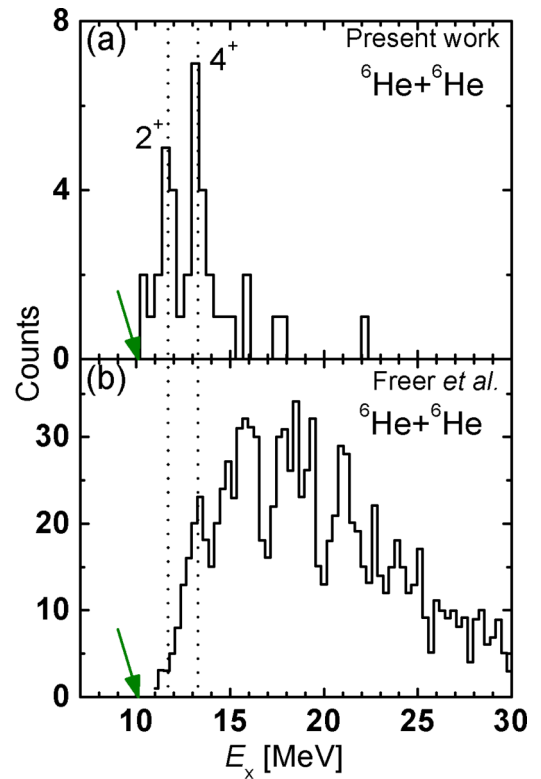


FIG. 4. (Color online) (a) The excitation energy spectrum for ^{12}Be , reconstructed from the $^6\text{He} + ^6\text{He}$ channel. (b) Data reported in Ref. [33]. The green (gray) arrow indicates the respective cluster decay threshold, and the vertical black-dotted lines are used to guide the peak positions.

A. Resonant states

The excitation energy (E_x) spectra for ^{12}Be are reconstructed from the $^6\text{He} + ^6\text{He}$ and $^4\text{He} + ^8\text{He}$ decay channels, as presented in Figs. 4 and 5, respectively.

1. $^6\text{He} + ^6\text{He}$ channel

For the $^6\text{He} + ^6\text{He}$ decay channel, although the number of counts recorded in the present experiment is quite limited (Fig. 4), two peaks at 11.7 and 13.3 MeV are clearly observed. The width (FWHM) of each peak is about 1 MeV, consistent with the simulated resolution of about 0.8 MeV [43]. The 13.3-MeV state agrees with the 13.2-MeV state reported by Freer *et al.*, which was assigned a spin-parity value of 4^+ based on an angular correlation analysis [33]. A new peak at 11.7 MeV is observed in the present experiment thanks to the high efficiency of our detection system at E_x close to the corresponding cluster separation threshold (Fig. 2). Following the systematics of the molecular rotational band proposed by Freer *et al.* [32], a spin parity of 2^+ might be assigned to this state (Fig. 4). Indeed we have verified the spin-parity assignments for these two peaks, by using calculations based on the distorted wave Born approximation (DWBA). The experimental angular distributions for these two excited states are found consistent with 4^+ and 2^+ spin-parity assignments, respectively, although the statistical error is quite large. The projected

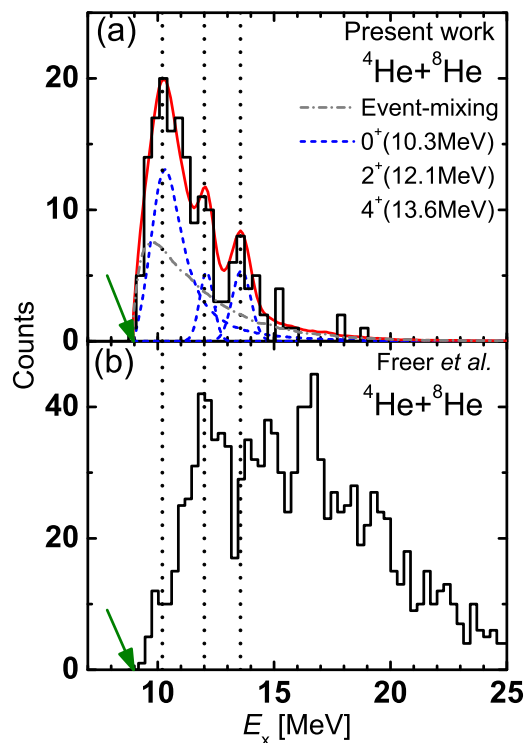


FIG. 5. (Color online) (a) The excitation energy spectrum for ^{12}Be , reconstructed from the $^4\text{He} + ^8\text{He}$ channel, together with the fit functions. (b) Data reported in Ref. [33]. The green (gray) arrow indicates the respective cluster decay threshold, and the vertical black dotted lines are used to guide the peak positions.

bandhead state (0^+) should be at an E_x of about 10.0 MeV, which is very close to the $^6\text{He} + ^6\text{He}$ separation threshold (10.1 MeV). As a matter of fact a few events do appear just above the threshold (Fig. 4). Considering the extremely low detection efficiency in this E_x region, these events give a good hint of the 0^+ bandhead state. A concrete observation of this state based on more delicate detection techniques should be important in completing this $^6\text{He} + ^6\text{He}$ molecular rotational band.

2. $^4\text{He} + ^8\text{He}$ channel

The $^4\text{He} + ^8\text{He}$ channel comprises a relatively large number of counts and therefore allows a more comprehensive analysis. Figure 5 presents the reconstructed E_x spectrum for the $^4\text{He} + ^8\text{He}$ decay channel. Three peaks at about 10.3, 12.1, and 13.6 MeV can be identified. The 12.1-MeV peak agrees exactly with that reported by Freer *et al.* [33]. The 13.6-MeV peak is also in consistency with the 14.1-MeV state observed by Freer *et al.* [33], considering the energy resolution around this state. A new and remarkably large peak stands around 10.3 MeV in Fig. 5. We note that our detection system covers an angular range of 0 – 12° , while that for Freer’s experiment is 2 – 24° . Accordingly, our detection efficiency around the 10.3-MeV peak is about five times larger than that for Freer’s experiment, but both become equal at $E_x \sim 13.5$ MeV, as illustrated in Fig. 2. Therefore, the spectrum shapes in Figs. 5(a) and 5(b) are indeed consistent with each other and an enhanced peak at ~ 10 MeV can also be expected in the latter [Fig. 5(b)], after

accounting for the difference in the detection efficiency. As a matter of fact, a “shoulder” at around 10.2 MeV was noticed by Charity *et al.* in the measurements with both hydrogen and carbon targets [34], which is in close resemblance to the large peak observed here when scaled by the detection efficiency. Excited states at ~ 10 MeV were also reported from a proton inelastic scattering experiment by Korshennikov *et al.* [35] and from a transfer experiment by Bohlen *et al.* as well [37]. There is also a hint of a wide peak at around 10 MeV in the E_x spectrum measured by Saito *et al.* [36], although beneath it is seen a high background, possibly due to the high incident energy (see discussions in Subsec. B below).

As indicated in many studies, the direct (nonresonant) breakup or phase-space distribution must be accounted for when analyzing resonant states lying close to the corresponding decay threshold [45]. This process is generally modeled with the “event mixing” technique [47] or the phase space analysis [45]. A function composed of three peaks together with the “event mixing” component is used to fit the experimental excitation energy spectrum, as shown in Fig. 5(a). We adopt a Breit-Wigner (BW) shape [40] for the first peak at around 10.3 MeV in order to extract the decay width of this resonant state, which is to be compared to the theoretical prediction [24]. This BW function was convoluted with the energy response function (Fig. 1(a) in Ref. [43]) and filtered by the acceptance (Fig. 2) before being used in the fitting procedure. A simple Gaussian function shape was used for the two peaks located at 12.1 and 13.6 MeV, the widths of which were set equal to the corresponding detection resolutions (Fig. 1(a) in Ref. [43]). From a least-square fitting, a width of 1.5(2) MeV is extracted for the 10.3-MeV peak, which characterizes its excitation and decay properties [17].

According to GTCM predictions for the $^4\text{He} + ^8\text{He}$ molecular rotational band, spin parities of 0^+ , 2^+ , and 4^+ might be tentatively assigned to the 10.3, 12.1, and 13.6 MeV states, respectively [22,24]. The angular distribution for the 13.6-MeV state was compared to the DWBA calculation and a reasonable consistency with the 4^+ assignment was indeed found, whereas that for the 10.3-MeV state is well characterized by the spin-0 expectation (see Fig. 9 in Sec. III C). But this kind of angular distribution analysis is infeasible for the 12.1-MeV state due to its low number of counts.

The 0^+ resonant state is of special importance to evaluate the monopole transition strength in ^{12}Be , which well serves to signal the cluster formation [19]. Therefore, the model-independent angular correlation analysis method [32] is employed in order to unambiguously determine the spin parity of the 10.3-MeV state. The angular correlation analysis of reaction products, based on the distribution of the reaction yields with respect to the center of mass (c.m.) emission angle (Ψ) of the fragment, is a robust method in determining the spin of a resonant state. This correlation is independent of the population procedure and therefore free from uncertainties in the optical potentials and from influences of the reaction mechanisms. This method has been discussed in detail by Freer *et al.* and successfully applied in the previous works [32,46]. For a resonant state with an angular momentum J , which subsequently breaks up into two spin-0 fragments, the angular correlation spectrum is proportional to $|P_J(\cos(\Psi))|^2$.

In the case of $J > 0$, the inelastically scattering angle θ^* (laboratory frame) of the nucleus will introduce deviations in the correlation pattern away from the ideal $|P_J(\cos(\Psi))|^2$ distribution. This effect can be corrected by modifying Ψ with a factor of $\frac{l_i - J}{J} \theta^*$ in order to project onto the $\theta^* = 0$ axis, with l_i the entrance channel angular momentum [32,46]. However, for small angle scattering, this modification does not strongly affect the angular correlation spectrum [32]. In addition, this correction is not necessary for $J = 0$, as it corresponds to the isotropic decay in the c.m. frame of the resonant state. Since $|P_J(\cos(\Psi))|^2$ is symmetric about $\Psi = \pi/2$ or $\cos(\Psi) = 0$, i.e., $|P_J(\cos(\Psi))|^2 = |P_J(\cos(\pi - \Psi))|^2$, the current analysis is thus performed for $|\cos(\Psi)|$ in order to have a better statistical presentation (experimental distributions were checked for the two Ψ ranges of $0 \sim \pi/2$ and $\pi/2 \sim \pi$, and no apparent difference was found). The uncertainty in $\cos(\Psi)$ is around 0.1 in average, determined from the Monte Carlo simulation, taking into account the detector resolutions.

We first analyzed the $|\cos(\Psi)|$ distribution for the 13.6-MeV state (Fig. 5). As can be seen in Fig. 6, the oscillatory behavior of the experimental spectrum is well reproduced by the simulation assuming spin 4, a value predicted within the GTCM approach [22,24]. This is a good demonstration of the validity and accuracy of the angular correlation method in the present work. We note that in the simulation the detection efficiency and resolutions of the detector system have been included.

The angular correlation data for the 10.3-MeV state (gated on E_x of 10.0–11.4 MeV [18]) are shown in Fig. 7 and compared with simulations assuming spin 0, 1, and 2. The experimental distribution clearly contradicts the components of spin 1 and 2 (and higher spins with more oscillations) but agrees nicely with the spin-0 component. The loss of events in the experimental distribution and the drop down of the simulated curves at $|\cos(\Psi)| \sim 1$ ($\Psi \sim 0^\circ$) can be attributed to the ineffectiveness of the coincident measurement for two adjacent fragments which move into the same CsI(Tl) crystal. We have also investigated the effect of the detector position resolution on the sensitivity of the angular correlation method. Simulations with uncertainties in $|\cos(\Psi)|$ ranging from 0.1 to 0.5 were carried out. It was found that spins 0, 1, and

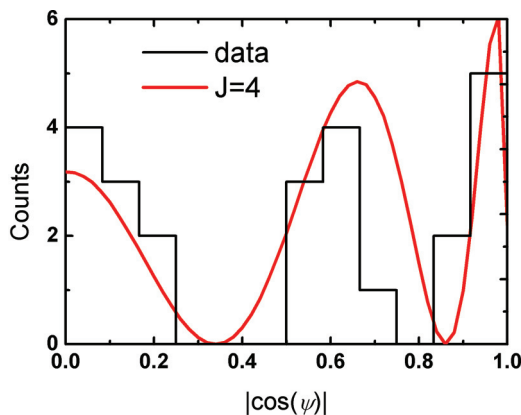


FIG. 6. (Color online) Angular correlation distribution for the 13.6-MeV state decaying into the $^4\text{He} + ^8\text{He}$ channel, compared with the simulation assuming $J = 4$ (red [gray] solid line).

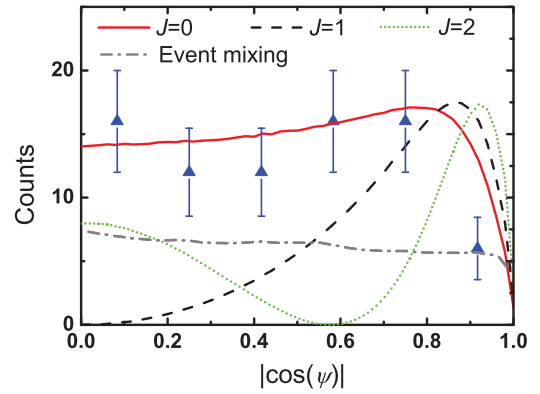


FIG. 7. (Color online) The angular correlation data (solid triangles) for the 10.3-MeV state decaying into the $^4\text{He} + ^8\text{He}$ channel. Simulations assuming $J = 0$ (red [gray] solid line), $J = 1$ (black dashed line), and $J = 2$ (green [gray] dotted line) are also presented for comparison. The simulated distributions have been smeared by the detector resolutions and filtered by the detection efficiency of the telescope.

2 can be well distinguished from each other even for an uncertainty in $|\cos(\Psi)|$ as large as 0.4, which largely exceeds the experimental value (~ 0.1 for most of $|\cos(\Psi)|$ range). Furthermore, to justify the purity of the broad 10.3-MeV peak, the same kind of angular correlation analyses were carried out by gating on E_x at either the left or right side of the peak. The resulting correlation distributions look similar to that in Fig. 7, indicating a pure spin-0 resonance.

B. Rotational bands

A number of cluster models have been applied to investigate molecular-like states in ^{12}Be , such as the AMD [30,48], GCM [31], and GTCM [22–24]. The GTCM calculations, based on a preformed α - $4n$ - α cluster structure, have successfully described both the low-lying molecular orbital states and the MR states above the cluster decay threshold. In particular two molecular rotational bands associated with the $^6\text{He} + ^6\text{He}$ and $^4\text{He} + ^8\text{He}$ binary systems were predicted [22].

The E_x of the resonant states in ^{12}Be are plotted against $J(J+1)$ for both $^4\text{He} + ^8\text{He}$ and $^6\text{He} + ^6\text{He}$ configurations in Fig. 8. Our data for the 2^+ and 4^+ states in the $^4\text{He} + ^8\text{He}$ band and the 4^+ state in the $^6\text{He} + ^6\text{He}$ band are in good agreement with Freer's results. And two states, namely the 0^+ state in the $^4\text{He} + ^8\text{He}$ band and the 2^+ state in the $^6\text{He} + ^6\text{He}$ band, are new observations of the present work, owing to the high detection efficiency at small E_{rel} (Fig. 2). These new findings provide apparent confirmation on the $^4\text{He} + ^8\text{He}$ and $^6\text{He} + ^6\text{He}$ molecular rotational bands proposed by Freer *et al.* and Ito *et al.* [22,32,33]. The GTCM calculation reproduces very well the experimental data (Fig. 8), although an overall shift of about 1.5 MeV is observed for the $^6\text{He} + ^6\text{He}$ band, compared with the experimental data. This discrepancy is approximately equal to the difference of 1.7 MeV between the experimental threshold energy and that from GTCM calculation and may be attributed to the adopted effective interaction strength [23].

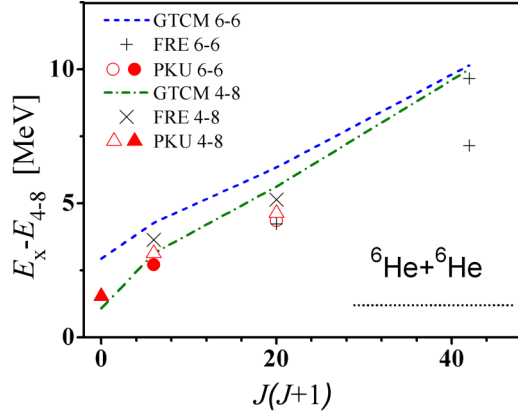


FIG. 8. (Color online) Energy-spin systematics for resonant states in ^{12}Be associated with the $^4\text{He} + ^8\text{He}$ and $^6\text{He} + ^6\text{He}$ configurations. The vertical axis is defined with respect to the separation energy of the $^4\text{He} + ^8\text{He}$ channel (E_{4-8}). The black short-dotted line at the right bottom indicates the decay threshold for the $^6\text{He} + ^6\text{He}$ channel. The $^4\text{He} + ^8\text{He}$ and $^6\text{He} + ^6\text{He}$ bands proposed from the GTCM calculations [22] are shown as the green (gray) dash-dotted line and the blue (gray) dashed line, respectively. The labeled symbols represent the experimental data obtained by Freer *et al.* [33] (FRE) and from the present work (PKU).

A small $\hbar^2/2\Theta$ value of about 0.15 MeV is obtained for the two rotational bands presented in Fig. 8, with Θ being the moment of inertia. This value is about 3 times smaller than that of the ground-state band in ^{10}Be (~ 0.5 MeV) [49] and is close to its $K^\pi = 0_2^+$ band (~ 0.18 MeV) associated with a well-developed cluster configuration [50]. As discussed in Sec. I, a large value of Θ is linked with a strong deformation and therefore signals the possible cluster formation in the nucleus. The good agreement between the experimental data and the GTCM calculation [22], based on the α - $4n$ - α cluster structure, for both $^4\text{He} + ^8\text{He}$ and $^6\text{He} + ^6\text{He}$ rotational bands provides strong support for a highly clustering structure in ^{12}Be .

It should be noted that the sensitivity of the breakup experiment to the cluster structure may depend on the collision energy, as tentatively discussed in Ref. [34]. As a matter of fact, this subject has been studied within the AMD approach [51]. It is found that the relative magnitude of the nonresonant direct breakup component enhances significantly with increasing incident energy, and becomes dominating when the incident energy exceeds 50 MeV/nucleon [51]. An optimal energy range of 20–30 MeV/nucleon is suggested for the investigation of the cluster structure in excited light nuclei [51]. A high background was indeed manifested in the reconstructed E_x spectrum for ^{12}Be , obtained from an inelastic excitation experiment at 60 MeV/nucleon [36,52]. Therefore, in the present work our results are mainly compared to those from Freer's experiment at a similar incident energy range.

From the present measurement, a considerably large width ($\Gamma = 1.5(2)$ MeV) is determined for the band head (10.3 MeV) of the $^4\text{He} + ^8\text{He}$ band (see Sec. III A 2), whereas other members in this band seem much narrower. This behavior of the resonances is indeed predicted by the GTCM calculations as shown in Fig. 3 of Ref. [18]. An enlarged width for

the cluster bandhead, located just above the corresponding decay threshold, was also suggested by the AMD calculations, considering the effects of the centrifugal barrier and the spin alignment [30]. From the above extracted large total width (1.5(2) MeV) and the experimentally determined cluster decay branching ratio, a cluster spectroscopic factor as large as 0.53(10) is deduced for the 10.3 MeV state [17], providing a strong support for the cluster formation in ^{12}Be .

It is worth noting that the negative-parity bands with the $^4\text{He} + ^8\text{He}$ configuration were also proposed in the AMD [30] and GCM [31] approaches, but not evidently observed in the present work (see Sec. III A). This may be ascribed to the weakening of the negative-parity states as discussed in Ref. [30].

C. Monopole transition strength

The monopole transition strength has been proposed as a sensitive probe for cluster formation in light nuclei [19,20,53]. Taking the Hoyle state in ^{12}C (0_2^+ at 7.65 MeV, with a 3- α structure) and the first two 0^+ excited states in ^{16}O (at 6.05 and 12.05 MeV, with a α - ^{12}C structure) as examples [20,54], the monopole transition matrix element ($M(E0)$) have been experimentally determined to be 5.4 ± 0.2 , 3.55 ± 0.21 , and 4.03 ± 0.09 fm², respectively. These values are comparable to the standard single-particle transition strength of ~ 5.4 fm² [54,55], which normally corresponds to much higher excitation energies. As a matter of fact, within a simple mean-field picture, the monopole excitation corresponds to a $2\hbar\omega$ jump of the single-particle orbits, for which an excitation energy of ~ 35 MeV should be required [19]. Accordingly, the monopole transition strength resulted from a mean-field calculation would hardly manifest itself in the E_x region below 20 MeV [20]. Instead, calculations based on cluster models, namely α - ^{12}C or 4- α structure in ^{16}O and 3- α structure in ^{12}C , may correctly reproduce the enhanced monopole transition strength mentioned above [20,54]. Therefore, the measurement of the enhanced monopole transition strength for excited states below 20 MeV would strongly signal the formation of cluster structure in light nuclei.

So far monopole transitions have been applied for cluster studies in light stable nuclei, by means of electromagnetic probes or hadron probes [55–57]. The electromagnetic probes, such as γ decay and electron scattering, are only sensitive to transitions associated with proton orbits, from which the electric transition strength can be extracted. On the other hand, the hadron probes, such as α or deuteron scattering, measure the isoscalar strength contributed from both proton and neutron orbits. The transition strength can be expressed in terms of the transition matrix element, $M(E0)$ or $M(\text{IS},0)$ for electric E0 or isoscalar monopole transition, respectively. These matrix elements are defined as [20]

$$M(E0) = \langle f | \sum_{i=1}^A \frac{1 + \tau_{3i}}{2} (\mathbf{r}_i - \mathbf{R}_{\text{c.m.}})^2 | \text{g.s.} \rangle, \quad (2)$$

$$M(\text{IS},0) = \langle f | \sum_{i=1}^A (\mathbf{r}_i - \mathbf{R}_{\text{c.m.}})^2 | \text{g.s.} \rangle,$$

where τ_3 is the isospin projection operator, and f and A are the final state and the mass number, respectively, of the nucleus. The energy-weighted sum rule (EWSR) for isoscalar transition $[S(\text{IS},0)]$ is expressed in the form [58,59]

$$S(\text{IS},0) = \sum_f |M(\text{IS},0)|^2 E_f = \frac{2\hbar^2}{m} A R_{\text{rms}}^2 \quad (3)$$

with m being the nucleon mass and R_{rms} being the root-mean-square matter radius of the nucleus.

For light α -conjugate nuclei, such as ^{12}C , ^{16}O , and ^{24}Mg , the density distributions for protons and neutrons are, to a good approximation, identical to each other, and therefore the protons and neutrons make almost identical contributions to the transition strength. The relation $M(E0) = \frac{1}{2}M(\text{IS},0)$ is thus well satisfied, and the $M(\text{IS},0)$ obtained from the alpha scattering measurements can be transferred to the $M(E0)$, as frequently adopted in the literature [56,57]. Accordingly, $S(E0)$ can be related to $S(\text{IS},0)$ via

$$S(E0) = \frac{1}{4}S(\text{IS},0) = \frac{\hbar^2}{2m} A R_{\text{rms}}^2. \quad (4)$$

It should be noted that for nuclei with large neutron-proton asymmetry, the transition strengths associated with the protons and neutrons are quite different because of their different density distributions. The simple scaling between $M(E0)$ and $M(\text{IS},0)$ with a factor of Z/A is thus not applicable [60]. Hence in the present work for ^{12}Be the discussions will be focused on the isoscalar strength ($M(\text{IS},0)$) only.

The isoscalar monopole transition is generally treated in the framework of a breathing mode oscillation, which can be analyzed within the optical model approach [58,61]. The associated transition potential, $G_0(r)$, can be expressed in terms of the standard optical potential $U(r)$ [61]:

$$G_0(r) = -\alpha_0^U \left[3U(r) + r \frac{dU(r)}{dr} \right], \quad (5)$$

where α_0^U is the potential amplitude parameter. For a state with an excitation energy of E_x that exhausts the EWSR, the amplitude of the transition density, α_0^m , is given by [58,59]

$$(\alpha_0^m)^2 = \frac{\hbar^2}{2m} \frac{4\pi}{A E_x} \frac{1}{R_{\text{rms}}^2}, \quad (6)$$

α_0^U is often related to α_0^m by equating deformation length [59]:

$$\delta_0 = \alpha_0^U R_U = \alpha_0^m c, \quad (7)$$

with c being the radius of the Fermi-type matter density distribution of the ground state of the nucleus being excited, and R_U being the radius of the real part of the Woods-Saxon-type optical potential.

Experimental determination of the transition matrix element can be achieved by carrying out the multipole-decomposition (MD) analysis of the inelastic differential cross sections in the form of [62,63]

$$\left(\frac{d\sigma}{d\Omega} \right)_{\text{exp}} = \sum_L a_L \left(\frac{d\sigma}{d\Omega} \right)_{L,\text{DWBA}}. \quad (8)$$

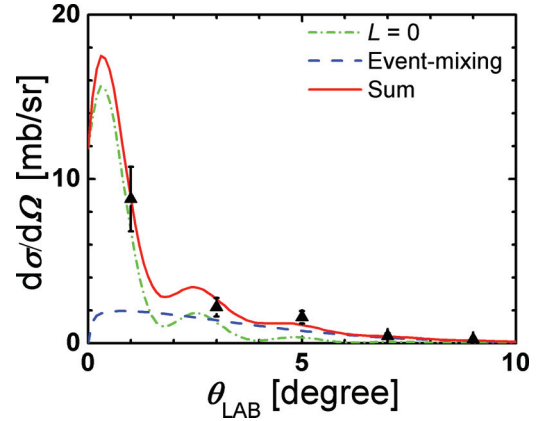


FIG. 9. (Color online) Experimental differential cross sections compared with the DWBA calculations for the 10.3-MeV state in ^{12}Be , populated in the inelastic scattering off a carbon target at 29 MeV/nucleon.

where $\left(\frac{d\sigma}{d\Omega} \right)_{\text{exp}}$ is the experimental data and $\left(\frac{d\sigma}{d\Omega} \right)_{L,\text{DWBA}}$ is the cross section calculated under the distorted wave Born approximation (DWBA) for a transferred angular momentum L , a_L , which can be extracted from a fitting procedure, corresponding to the fraction of the EWSR for a monopole ($L=0$) or a multipole ($L \geq 1$) transition. It should be noted that when studying the transitions from the 0^+ g.s. of the projectile off an adiabatic spin-0 target, the transferred angular momentum L is equal to the spin J of the final excited state.

The monopole transition strength for the 10.3-MeV state in ^{12}Be can then be determined from the experimental differential cross sections as plotted in Fig. 9. An E_x gate of 10.0–11.4 MeV is applied to reduce the nonresonant background and contaminations from the low-energy tail of the 2^+ and 4^+ states. The $^{12}\text{Be} + ^{12}\text{C}$ optical potential is taken from the analysis of the $^{12}\text{C} + ^{12}\text{C}$ scattering at 30 MeV/nucleon [64]. With $R_{\text{rms}} = 2.59(6)$ fm [65], an α_0^m value of 0.56 can be deduced from Eq. (6) for a state at $E_x = 10.3$ MeV which exhausts 100% of the EWSR limit. Since $c = 1.65$ fm is fixed from the ^{12}Be matter density distribution [66], an α_0^U value of 0.10 can then be deduced, following Eq. (7) and discussions made by Satchler [58]. As discussed in Sec. III A 2, within the applied E_x range of 10.0–11.4 MeV, the E_x spectrum is dominated by a high-purity 0^+ state with negligible contaminations from states with higher spins. Therefore, in the present work, only an $L=0$ component and a background modeled by the “event-mixing” technique are taken into account in the above described MD analysis [Eq. (8)]. The DWBA calculation was performed using the code FRESKO [67] and the resulting cross section was convoluted with the experimental angular resolution and multiplied by the acceptance of the detection system. Based on a Monte Carlo simulation, the angular resolution (FWHM) is determined to be ~ 0.35 deg, contributed from uncertainties in determining the reaction position and the position and energy of the fragments.

As shown in Fig. 9, the experimental differential cross sections are well reproduced by the DWBA calculations with a normalization factor $a_0 = 0.034(10)$, which is associated with the fraction of the EWSR. The applied E_x gate rejects a portion

of events which belong to the 0^+ state (10.3 MeV). This can be recovered by using the above obtained BW function (Fig. 5) and the corrected fraction is then 0.075(24). According to Eq. (3) the corresponding EWSR is $6727.9 \text{ fm}^4 \text{ MeV}^2$, and the deduced monopole transition matrix element ($M(\text{IS})$) is $7.0 \pm 1.0 \text{ fm}^2$. The error of $M(\text{IS})$ quoted here is statistical only. The systematic error is estimated to be about 12%, contributed mainly from the uncertainties in the DWBA calculation and the modeling of the shapes of the 10.3-MeV peak and the event-mixing background.

The currently extracted $M(\text{IS})$ for the 10.3-MeV state is comparable to those for the typical cluster states in ^{12}C and ^{16}O as noted above [54,55]. Recently, the monopole transitions in ^{12}Be have been extensively studied by Ito *et al.* within the GTCM approach assuming a preformed α - $4n$ - α configuration [19,22]. In their calculation five 0^+ excited states were predicted with excitation energies below 20 MeV [19]. Especially the 0_3^+ state at ~ 10 MeV, with a dominating $^4\text{He} + ^8\text{He}$ cluster configuration, possesses an extremely large monopole transition strength of $\sim 10 \text{ fm}^2$ (the cluster part) [19]. This is in close agreement with our present observation. We notice that the 10.3-MeV state analyzed here is reconstructed from the $^4\text{He} + ^8\text{He}$ decay channel only. Hence the obtained $M(\text{IS}) = 7.0 \pm 1.0 \text{ fm}^2$ should be regarded as the lower limit. A better agreement between the calculation and the measurement should be expected after accounting for other possible cluster decay channels [68].

IV. SUMMARY

In summary, we have carried out an inelastic breakup experiment with a ^{12}Be beam at 29 MeV/nucleon off a

carbon target. From coincident measurements of the decay fragments, the excitation energy spectra are reconstructed for the $^6\text{He} + ^6\text{He}$ and $^4\text{He} + ^8\text{He}$ decay channels. Two resonant peaks are clearly identified in the $^6\text{He} + ^6\text{He}$ decay channel and three for $^4\text{He} + ^8\text{He}$, with the lowest-lying ones in both channels being the new observations. A remarkably large peak at 10.3 MeV in the $^4\text{He} + ^8\text{He}$ channel was observed thanks to the large detection efficiency at excitation energies close to the respective cluster separation threshold. Using the model-independent angular correlation analysis, a pure 0^+ spin parity can be assigned to this state, providing direct confirmation on the previously proposed molecular rotational band. From the analysis of the angular distribution associated with this state, a largely enhanced monopole transition matrix element ($M(\text{IS})$) of $7.0 \pm 1.0 \text{ fm}^2$ is obtained, which is comparable to those for typical cluster states in ^{12}C and ^{16}O . Combined with the large cluster spectroscopic factor of 0.53(10) reported in our previous publication, all findings from the present experiment consistently evidence a well-developed cluster state in ^{12}Be . The present work demonstrates, for the first time, that the monopole transition strength is a promising tool to signal the cluster formation in unstable nuclei. The zero-deg telescope, in favor of detecting the states with small decay energies, played an essential role in this experiment.

ACKNOWLEDGMENTS

The technical and operational support of the staff at HIRFL-RIBLL is gratefully acknowledged. The authors have benefited from discussions with M. Ito, M. Freer, Y. H. Zhang, and X. H. Zhou. This work is supported by the 973 Program of China (No. 2013CB834402) and NSFC (Projects No.11035001, No. 11275011, No. 11275001, and No. J1103206).

-
- [1] J. A. Wheeler, *Phys. Rev.* **52**, 1107 (1937).
 - [2] L. R. Hafstad and E. Teller, *Phys. Rev.* **54**, 681 (1938).
 - [3] H. Geiger, *Z. Phys.* **8**, 45 (1922).
 - [4] H. J. Rose and G. A. Jones, *Nature (London)* **307**, 245 (1984).
 - [5] W. von Oertzen, M. Freer, and Y. Kanada-En'yo, *Phys. Rep.* **432**, 43 (2006).
 - [6] W. N. Catford, *J. Phys. Conf. Series* **436**, 012085 (2013).
 - [7] M. Chernykh, H. Feldmeier, T. Neff, P. von Neumann-Cosel, and A. Richter, *Phys. Rev. Lett.* **98**, 032501 (2007).
 - [8] K. Ikeda, N. Tagikawa, and H. Horiuchi, *Prog. Theor. Phys. Suppl.* **E68**, 464 (1968).
 - [9] K. Ikeda, H. Horiuchi, and S. Saito, *Prog. Theor. Phys. Suppl.* **68**, 1 (1980).
 - [10] K. Hagel *et al.*, *Phys. Rev. Lett.* **108**, 062702 (2012).
 - [11] Y. L. Ye *et al.*, *Chin. Phys. C* **36**, 127 (2012).
 - [12] H. Horiuchi, *J. Phys. Conf. Series* **436**, 012003 (2013).
 - [13] P. G. Hansen and B. Jonson, *Euro. Phys. Lett.* **4**, 409 (1987).
 - [14] Y. Kanada-En'yo, M. Kimura, A. Ono, *Prog. Theor. Exp. Phys.* (2012) 01A202.
 - [15] K. A. Erb and D. A. Bromley, *Treatise of Heavy-Ion Science 3* (Plenum, New York, 1985), p. 201.
 - [16] M. Freer and A. C. Merchant, *J. Phys. G: Nucl. Part. Phys.* **23**, 261 (1997).
 - [17] Z. H. Yang *et al.*, *Sci. China-Phys. Mech. Astron.* **57**, 1613 (2014).
 - [18] Z. H. Yang *et al.*, *Phys. Rev. Lett.* **112**, 162501 (2014).
 - [19] M. Ito, *Phys. Rev. C* **83**, 044319 (2011).
 - [20] T. Yamada, Y. Funaki, T. Myo, H. Horiuchi, K. Ikeda, G. Ropke, P. Schuck, and A. Tohsaki, *Phys. Rev. C* **85**, 034315 (2012).
 - [21] N. Itagaki and S. Okabe, *Phys. Rev. C* **61**, 044306 (2000).
 - [22] M. Ito, N. Itagaki, H. Sakurai, and K. Ikeda, *Phys. Rev. Lett.* **100**, 182502 (2008).
 - [23] M. Ito, N. Itagaki, and K. Ikeda, *Phys. Rev. C* **85**, 014302 (2012).
 - [24] M. Ito, *Phys. Rev. C* **85**, 044308 (2012).
 - [25] A. Navin *et al.*, *Phys. Rev. Lett.* **85**, 266 (2000).
 - [26] S. D. Pain *et al.*, *Phys. Rev. Lett.* **96**, 032502 (2006).
 - [27] H. T. Fortune, G. B. Liu, and D. E. Alburger, *Phys. Rev. C* **50**, 1355 (1994).
 - [28] H. Iwasaki *et al.*, *Phys. Lett. B* **491**, 8 (2000).
 - [29] N. Itagaki, S. Okabe, and K. Ikeda, *Phys. Rev. C* **62**, 034301 (2000).
 - [30] Y. Kanada-En'yo and H. Horiuchi, *Phys. Rev. C* **68**, 014319 (2003).
 - [31] M. Dufour, P. Descouvemont, and F. Nowacki, *Nucl. Phys. A* **836**, 242 (2010).
 - [32] M. Freer *et al.*, *Phys. Rev. Lett.* **82**, 1383 (1999).
 - [33] M. Freer *et al.*, *Phys. Rev. C* **63**, 034301 (2001).

- [34] R. J. Charity *et al.*, *Phys. Rev. C* **76**, 064313 (2007).
- [35] A. A. Korshennikov *et al.*, *Phys. Lett. B* **343**, 53 (1995).
- [36] A. Saito *et al.*, *Nucl. Phys. A* **738**, 337 (2004).
- [37] H. G. Bohlen, W. von Oertzen, T. Kokalova, C. Schulz, R. Kalpakchieva, T. N. Massey, and M. Milin, *Int. J. Mod. Phys. E* **17**, 2067 (2008).
- [38] Z. Sun *et al.*, *Nucl. Instrum. Meth. A* **503**, 496 (2003).
- [39] R. Qiao *et al.*, *IEEE Trans. Nucl. Sci.* **61**, 596 (2014).
- [40] Z. X. Cao *et al.*, *Phys. Lett. B* **707**, 46 (2012).
- [41] L. H. Lv *et al.*, *Chin. Phys. C* **35**, 891 (2011).
- [42] L. H. Lv *et al.*, *J. Phys. G: Nucl. Part. Phys.* **39**, 065102 (2012).
- [43] Z. H. Yang and Y. L. Ye, *EPJ Web Conf.* **66**, 02112 (2014).
- [44] N. I. Ashwood *et al.*, *Phys. Lett. B* **580**, 129 (2004).
- [45] A. Spyrou *et al.*, *Phys. Rev. Lett.* **108**, 102501 (2012); **109**, 239202 (2012).
- [46] M. Freer, *Nucl. Instrum. Meth. A* **383**, 463 (1996).
- [47] M. Assie *et al.*, *Eur. Phys. J. A* **42**, 441 (2009).
- [48] Y. Kanada-En'yo, H. Horiuchi, and A. Ono, *Phys. Rev. C* **52**, 628 (1995).
- [49] W. von Oertzen, *Z. Phys. A* **357**, 355 (1997).
- [50] M. Freer *et al.*, *Phys. Rev. Lett.* **96**, 042501 (2006).
- [51] H. Takemoto, H. Horiuchi, and A. Ono, *Phys. Rev. C* **63**, 034615 (2001).
- [52] A. Saito *et al.*, *Mod. Phys. Lett. A* **25**, 1858 (2010).
- [53] H. Horiuchi, K. Ikeda, and K. Kat, *Prog. Theor. Phys. Suppl.* **192**, 1 (2012).
- [54] T. Yamada, Y. Funaki, H. Horiuchi, K. Ikeda, and A. Tohsaki, *Prog. Theor. Phys.* **120**, 1139 (2008).
- [55] P. Ajzenberg-Selove, *Nucl. Phys. A* **460**, 1 (1986).
- [56] D. H. Youngblood, Y.-W. Lui, and H. L. Clark, *Phys. Rev. C* **57**, 2748 (1998).
- [57] Y.-W. Lui, H. L. Clark, and D. H. Youngblood, *Phys. Rev. C* **64**, 064308 (2001).
- [58] G. R. Satchler, *Nucl. Phys. A* **472**, 215 (1987).
- [59] D. J. Horen, J. R. Beene, and G. R. Satchler, *Phys. Rev. C* **52**, 1554 (1995).
- [60] G. R. Satchler, *Nucl. Phys. A* **540**, 533 (1992).
- [61] G. R. Satchler and D. T. Khoa, *Phys. Rev. C* **55**, 285 (1997).
- [62] M. Itoh *et al.*, *Phys. Lett. B* **549**, 58 (2002).
- [63] D. H. Youngblood, H. L. Clark, and Y.-W. Lui, *Phys. Rev. Lett.* **82**, 691 (1999).
- [64] M. Buenerd, A. Lounis, J. Chauvin, D. Leberun, P. Martin, G. Duhamel, J. C. Gondrand, and P. De Saintignon, *Nucl. Phys. A* **424**, 313 (1984).
- [65] A. Ozawa, T. Suzuki, and I. Tanihata, *Nucl. Phys. A* **693**, 32 (2001).
- [66] S. Ilieva *et al.*, *Nucl. Phys. A* **875**, 8 (2012).
- [67] I. J. Thompson, *Comput. Phys. Rep.* **7**, 167 (1988).
- [68] M. Ito and K. Ikeda, *Rep. Prog. Phys.* **77**, 096301 (2014).